



HAL
open science

From sintering to particle discrimination: New opportunities in Metal-Organic Frameworks scintillators

Vincent Villemot, Nicolas Dufour, Sharvane Mauree, Benoit Sabot,
Guillaume Bertrand, Matthieu Hamel

► To cite this version:

Vincent Villemot, Nicolas Dufour, Sharvane Mauree, Benoit Sabot, Guillaume Bertrand, et al.. From sintering to particle discrimination: New opportunities in Metal-Organic Frameworks scintillators. *Advanced Photonics Research*, 2021, pp.2100259. 10.1002/adpr.202100259 . cea-03442303

HAL Id: cea-03442303

<https://cea.hal.science/cea-03442303>

Submitted on 23 Nov 2021

HAL is a multi-disciplinary open access archive for the deposit and dissemination of scientific research documents, whether they are published or not. The documents may come from teaching and research institutions in France or abroad, or from public or private research centers.

L'archive ouverte pluridisciplinaire **HAL**, est destinée au dépôt et à la diffusion de documents scientifiques de niveau recherche, publiés ou non, émanant des établissements d'enseignement et de recherche français ou étrangers, des laboratoires publics ou privés.



Distributed under a Creative Commons Attribution 4.0 International License

1 **From sintering to particle discrimination: New opportunities in Metal-Organic**
2 **Frameworks scintillators**

3
4 *Vincent Villemot, Nicolas Dufour, Sharvane Mauree, Benoît Sabot, Guillaume H. V. Bertrand,*
5 *Matthieu Hamel*

6
7
8 V. Villemot*, N. Dufour, S. Mauree, Dr. B. Sabot, Dr. G. H. V. Bertrand, Dr. M. Hamel*
9 Université Paris Saclay, CEA, List, F-91120 Palaiseau, France.

10 vincent.villemot@cea.fr and matthieu.hamel@cea.fr

11 Orcid numbers: 0000-0002-9478-6651 (VV), 0000-0001-8551-709X (ND), 0000-0003-3043-
12 8006 (BS), 0000-0003-2061-9241 (GHVB), 0000-0002-3499-3966 (MH).

13
14 **Keywords:** MOF, scintillator, densification, photoluminescence, radioluminescence, MCNP,
15 discrimination

16
17 **Abstract:**

18 The characterization of a scintillating Metal Organic Framework (MOF) is not straightforward,
19 mainly due to the small size and low density of the material. In this context, we present herein
20 a generic method to give an easy access to the determination of a key parameter in the
21 scintillation field, namely the light output. To reach this, MOF-205 was first synthesized as
22 millimetric-size single crystals then sintered under pressure and temperature conditions to
23 afford a pellet. The density was increased by 300% while maintaining optical properties on par
24 with scintillation application. The as-prepared scintillator was then characterized in terms of
25 photoluminescence (UV-excited emission spectrum, time-correlated single photon counting)
26 and radioluminescence spectroscopy (beta-excited emission spectrum, alpha, beta and gamma
27 pulse height spectra, alpha/beta and alpha/gamma discrimination). Results were compared with
28 commercial BC-404 plastic scintillator performances as well as supported by MCNP6.2
29 simulation.

30
31 **1. Introduction**

32 Methods to detect, qualify and quantify ionizing radiations were introduced soon after the
33 discovery of radioactivity by Henri Becquerel in 1896. Currently, numerous applications benefit
34 from this field, ranging from nuclear activities, research in high-energy physics, astronomy,

35 homeland security and medicine. Depending on the radionuclide to be detected, various
36 disintegrations can occur, the most common and probable leading to the emission of alpha or
37 beta particles often followed by de-emissions producing X and/or gamma rays. These ionizing
38 radiations can be detected with scintillators, which are materials that are efficient to produce
39 light when exposed to such radiations. This specific class of photoluminescent materials is
40 divided into two main categories, namely inorganic and organic scintillators.^[1] The former
41 subclass appeared as early as 1895 (barium tetracyanoplatinate(II) $\text{BaPt}(\text{CN})_4$)^[2]. The later was
42 pioneered when the use of naphthalene was first reported in 1947.^[3] Since these seminal
43 publications, many efforts have been performed in the two chemistry worlds for the quest of
44 the 'best' scintillator. However, both have pros and cons and currently no photoluminescent
45 material represents the Holy Grail that could fulfil all requirement in terms of radiation
46 detection (among others: detection efficiency against production cost). In this context, scientists
47 have considered using advantages from both worlds, hence leading to a various range of
48 scintillators such as sol-gel, hybrid materials or nanoparticles-loaded plastics.^[4] Most
49 particularly, composite scintillators stand out as they can bypass a lot of limitations. The core
50 idea is to take a known efficient scintillator, mainly an organic or inorganic single crystal, and
51 embed them into a matrix of suitable polymer. This will give access to what can be described
52 as a polycrystalline scintillator. As single crystals are often hard to produce in large scale or are
53 not very stable towards ambient condition (mechanical weakness, humidity and temperature
54 dependency), this technology affords a way to combine large quantity of efficient scintillator
55 and stability-aimed encapsulation.

56 Metal organic frameworks (MOFs) are a class of hybrid materials.^[5] Under their crystalline
57 form, they have found great interest to many researchers in a wide variety of fields because of
58 their great versatility.^[6] They are constructed of inorganic nodes linked with each other by
59 organic ligands. Therefore, the modification of one or both bricks allows modifying the final
60 properties, the only limitation being thus the creativity of the scientist. Allendorf *et al.* were the

61 first to highlight the possibility to use MOFs as potent scintillators. They observed decent light
62 outputs (up to 22% of anthracene, ca. $3,300 \text{ ph}\cdot\text{MeV}^{-1}$) by switching traditional organic linkers
63 for a dicarboxylated *trans*-stilbene, an already known and efficient scintillating molecule.^[7]
64 Thanks to the above mentioned high degree of versatility of MOF construction, some
65 researchers, again using ligands based on scintillating molecules, have also assembled
66 frameworks based on traditional inorganic bricks and heavier metals to increase the stopping
67 power of X-rays. For example, Wang *et al.* have synthesized two different 9,10-di(*para*-
68 carboxyphenyl)anthracene (DPA)-based MOFs,^[8] where one was connected to Zr nodes
69 whereas the other to Hf nodes. As the two materials have different X-ray cross sections, it was
70 possible to show a qualitative increased sensitivity for Hf-MOF.

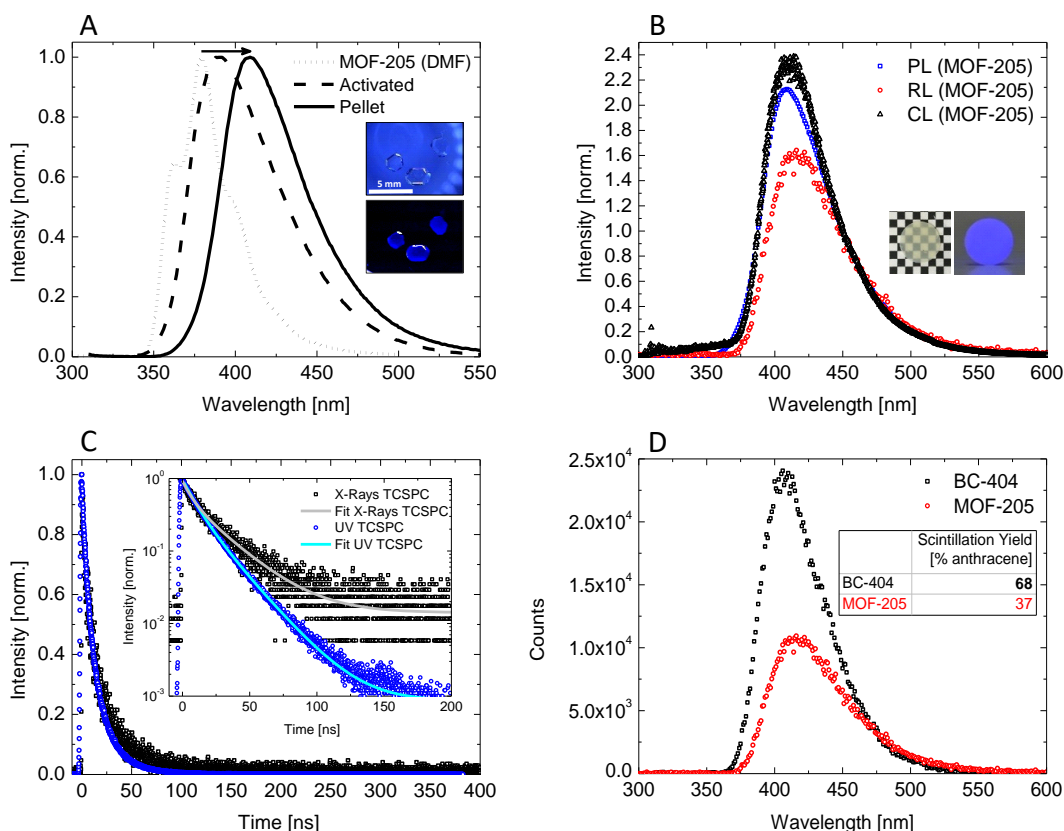
71 Recently, new contributions have emerged involving Metal-Organic Frameworks as
72 scintillators, having in mind their use in medical applications such as TOF-PET detectors.^[9]
73 Perego *et al.* have embedded the DPA-based Zr-MOF (previously synthesized by Wang^[8])
74 inside two polymeric matrices: poly(dimethylsiloxane) (PDMS) and poly(methyl methacrylate)
75 (PMMA). As MOFs can be hard to synthesize in large crystals, difficult to scale up and tricky
76 to handle, composite materials seem to be the go-to solution to test them as scintillators.
77 However, several limitations are foreseen with the incorporation of a MOF inside a matrix, and
78 in general to the characterization of MOFs as scintillators. Despite efforts by chemists to
79 synthesize MOF nanocrystals, these are subject to strong light scattering already at a low
80 percentage of incorporation in the polymer matrix, which can lead to turbidity observed at
81 loading as low as 0.5 weight%. This is mainly caused by the incorrect matching between the
82 matrix and MOFs refractive index which lead to light scattering. This effect coupled to the
83 numerous interfaces between the matrix and the embedded MOF can thus lead to strong
84 deviation from the optimal light collection. These cumulated factors are altering the global
85 optical properties and leading to a moderate scintillating material (6% the light output of
86 anthracene, which is ca. $1,000 \text{ ph}\cdot\text{MeV}^{-1}$). Other literature from this field generally describes

87 analytical methods that have to be adapted to small-size and low-density MOF materials, for
88 example with Ion Beam Induced Luminescence^[7] (IBIL) or small X-ray tubes,^[8]. This
89 experiments require high dose delivery^[8, 9] or tedious characterization in liquid suspension.^[8]
90 Such techniques are useful but developing a universal characterization method for scintillating
91 MOFs the closest to their final use, which means confronted to the presence of radionuclides
92 and without form factor (e.g. single crystals dispersed in a liquid) would be of great value for
93 the scientific community, and that was the core idea at the root of this study.

94 To overcome these issues, this work presents two major contributions leading to scintillating
95 materials made from MOFs. The first concerns the densification by sintering until translucent
96 media are reached.^[10] The second concerns the nearly transparent pellet entirely composed by
97 a luminescent MOF, and its use as scintillator. This application becomes particularly natural
98 and of practical use to determine one of the scintillator key parameter: the light output.
99 Experimental results, validated by particle radiation transport simulations performed with the
100 MCNP6.2 Monte Carlo code allowed for the first time to characterize a Metal Organic
101 Framework under alpha, beta and gamma excitation, and to observe a light output that can
102 compete with a commercial plastic scintillator (BC-404, Saint-Gobain Crystals and
103 Detectors^[11,12]). Furthermore the hybrid nature of our sintered MOF was put in the perspective
104 of classical inorganic and organic crystal scintillation. Those fields are known to demonstrate
105 good particle discrimination by PSD. This approach was applied to our materials and
106 unprecedented particle discrimination with scintillating MOFs has been reached, confirming
107 precedent hint from Allendorf *et al.*^[15]

108
109
110
111
112
113
114
115

116 2. Results and discussion



117

118 **Figure 1.** Structural and photophysical properties of sintered MOF-205. A) Photoluminescence
 119 spectra of MOF-205 in DMF (dotted line), activated (dashed line) and pellet (solid line). Inset
 120 are pictures of millimetric single crystals under visible light and under 365 nm excitation light.
 121 B) Normalized steady-state Photoluminescence (PL), Radioluminescence (RL) and
 122 Cathodoluminescence (CL) spectra of sintered MOF-205. Inset are pictures of pellet under
 123 visible light and under 365 nm excitation light (excitation source was placed behind the pellet).
 124 C) Time-Correlated Single Photon Counting (TCSPC) of sintered MOF-205 after 274 nm
 125 excitation (blue) and X-rays excitation (black). Decay values are the result of a biexponential
 126 fitting with a $R^2 = 0.99$. D) Radioluminescence spectra of BC-404 and MOF-205 (both are \varnothing
 127 13 mm and thickness 400 μm). Area integration allows to recover the scintillation efficiency
 128 values.

129 As demonstrated in many contributions, MOF synthesis is tricky and requires attention as an

131 impurity can have a large impact on the final photophysical properties.^[13] As a case study, we

132 chose a MOF where the secondary building unit is Zn_4O , linked with two different organic
 133 linkers: 1,3,5-tris(4-carboxyphenyl)benzene (H_3BTB) and 2,6-naphthalene dicarboxylate (2,6-

134 NDC), which is also named MOF-205 or DUT-6.^[14,15] It was selected as a potent candidate

135 thanks to its photoluminescent properties that comply with standard plastic scintillators: fast

136 decay time and emission wavelength centered around 420 nm. These interesting features are

137 carry by the naphthalene moiety, which is a well-known molecule in the scintillation field.^[16]
138 The second reason is that this framework presents a cubic lattice structure, which is compliant
139 with sintering application, a key in densification. Theoretically, under uniaxial pressure planes
140 of cubic structures should move isotropically and finally result in a material densification, a
141 result that would be less easy to achieve with non-cubic lattices^[10], or anisotropic collapses.
142 Here we propose a densification of MOF under two external stimuli: pressure and temperature.
143 This has already been demonstrated by Zacharia *et al.* only under the action of pressure for
144 MOF-177, a MOF that is similar to MOF-205.^[17] This trend remains marginal as the purpose
145 of synthesizing MOF is, classically, to use their porosity properties, which is not compatible
146 with densification.

147 Thus, MOF-205 was synthesized to obtain large, pure, millimeter-sized crystals (Inset of **Figure**
148 **1.A**), was sintered and fully characterized (see Supporting Information, Figure S1). As heat can
149 promote the plastic displacement leading to densification, temperature limits should be defined
150 in order to prevent any parasitic degradation of the (photo)physical properties. Thus, thermal
151 decomposition behavior was investigated in order to characterize its thermal stability. As shown
152 in Figure S2, thermogravimetric analysis (TGA) shows two characteristic weight losses. The
153 first continuous weight loss of 9.9% in the temperature range from 30 °C to 350 °C corresponds
154 to the desorption of guest molecules. The second drastic loss of 66.4% occurring at 450 °C
155 corresponds to the decomposition of the frameworks to ZnO and organic byproduct. From this
156 analysis, we decided to constrain the sintering to an operating window between 30 °C and
157 200 °C in order to avoid any deterioration of the MOF during this process. Thus, activated
158 powder of MOF-205 was pressed under 15 tons in a 13 mm diameter dye at 100 °C for 20 min,
159 corresponding to a pressure of 1.1 GPa. The resulting pellet (Inset of **Figure 1.B**) presented a
160 thickness of $400 \pm 20 \mu\text{m}$ and a mass of 82 mg. Considering the pellet as a perfect cylinder, a
161 density of 1.56 ± 0.08 was calculated, which represents a remarkable increase of 300%
162 compared to its original density (0.38).^[14] Furthermore, the resulting pellet displayed promising

163 photophysical properties. Main spectral characteristics were obtained from either UV
164 photoluminescence (PL) or ionizing radiation such as radioluminescence (RL) with an $^{90}\text{Sr}/^{90}\text{Y}$
165 beta source or cathodoluminescence (CL) with an X-ray excitation. The results are shown in
166 **Figure 1.A-D**, and discuss below.

167 At the origin of our composite scintillator, MOF-205 in DMF presents an emission of 380 nm
168 with characteristic vibronic structure of linker in its dilute form (**Figure 1.A**). This is
169 characteristic of a ligand-centered emission. As already mentioned in many publications,
170 frameworks are likely to be dependent on their environment, guest molecules or impurities
171 trapped inside their porosity. Fluorescence is especially sensitive to external stimuli when it
172 arises from the linker only as is the case for MOF-5 for example.^[18] Hence, upon activation the
173 material loses its fine structure and shows a Gaussian-type emission centered at higher
174 wavelengths (394 nm). Then after pressing, the pellet shows a slightly different steady-state
175 photoluminescence as the fluorescence maximum undergoes a shift to 409 nm (**Figure 1.B**).
176 This wavelength increase could be explained by larger π overlaps between the ligands due to
177 the densification of the material and the reduction of the ligands distance to each other. Thus,
178 the energy gap would be reduced and would result in a bathochromic shift at the image of the
179 ligand in its solid form ($\lambda_{\text{em}} = 452 \text{ nm}$) (Figure S3). This assumption is confirmed by a
180 comparison of the time-resolved fluorescence spectra. Under the effect of pressure and
181 temperature the material therefore tends to amorphise and favours a spatial rearrangement of
182 the ligands which leads to emission at a higher wavelength. This is confirmed as the pellet
183 shows no X-ray diffraction. This trend is as also demonstrated by Zacharia *et al.* for a similar
184 MOF.^[17] However, we assume that this structural change remains minor as the average lifetime
185 is only slightly changed compared to pure activated MOF-205 single crystal (Figure S4). This
186 results collectively show that MOF-205 as a single crystal or sintered as a pellet have the same
187 photophysical behavior. Sintered pellets are hence a good sudo-sample to judge the scintillation

188 response of a MOF. Pellets are also more practical to use and starting from this point, we are
189 considering the pellets as scintillating material in their own rights.

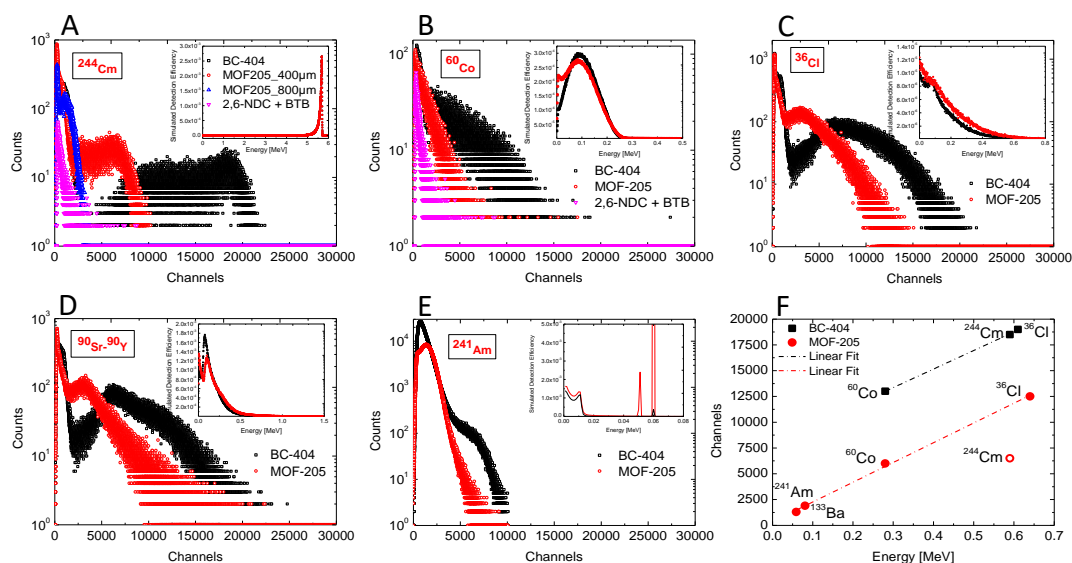
190 Radioluminescence (RL) and cathodoluminescence (CL), contrary to PL, allow the
191 investigation of excited states by ionization with radionuclides. As known, ionization process
192 is quite different from PL as ionization can lead to several changes in the electronic and
193 molecular structure of matter, thus expectable discrepancies in emission wavelength or/and in
194 lifetime. **Figure 1.B** compares normalized PL, RL and CL state spectra. Since RL and CL/PL
195 are recorded in transmission and front face, respectively, it is possible to notice several changes
196 in the shape of the Gaussian-type emission. This is mainly due to reabsorption and diffusion
197 occurring within the pellet. However, since traditional scintillation measurements are usually
198 performed in transmission, the RL experiment is closer to the application measurement method.
199 **Figure 1.C** represents the Time-Correlated Single Photon Counting (TCSPC) of sintered MOF-
200 205 after 274 nm excitation (blue) and X-rays excitation (black). It is interesting to note that
201 under X-rays excitation the pellet shows a fast and slow component in similar magnitudes as
202 under UV excitation. However, the weights of each components are different. Thus, the average
203 lifetime increases from 14.8 to 17.8 ns (Figure S5). This could be explained by a larger
204 population.

205 To highlight the use of sintered pellet of MOF-205, RL measurements were carried out with a
206 well-known reference in the scintillation field, namely BC-404 (Saint-Gobain Crystals and
207 Detectors) with same size and shape: a cylinder with 13 mm diameter and 400 μm thickness.
208 Both materials can thus be compared, provided that the experimental set up is identical as well.
209 This is shown in a radioluminescence experiments presented in **Figure 1.D**. As the area under
210 the curve corresponds to the amount of emitted photons, it is possible to estimate a scintillation
211 efficiency by a rule of thumb. MOF-205 emits 55% of what the BC-404 is capable. In other
212 words, this means that MOF-205 has a light output of 37% compared to anthracene, as the BC-

213 404 is 68% according to its datasheet.^[11] Considering that anthracene is $\approx 15,000 \text{ ph}\cdot\text{MeV}^{-1}$,
214 the light output of the sintered MOF-205 is thus around $5,500 \text{ ph}\cdot\text{MeV}^{-1}$. The above results
215 validate the concept of a sintered MOF-205 as an intrinsic scintillator and places it above other
216 MOF-based scintillators as far as light output is concerned.

217 As the pellets are quite thin, the use of alpha-emitting source is obvious in terms of
218 characterization with radionuclides. Alpha emitters have a short penetration distance in matter,
219 and therefore ionize the pellet by depositing all their energy as shown by simulation (Inset of
220 **Figure 2.A**). For instance, the alpha emitter ^{244}Cm presents two characteristics energy lines at
221 5.804 MeV (76.7%) and 5.762 MeV (23.3%).^[19] With this energy, alpha particles from ^{244}Cm
222 are fully stopped within $400 \mu\text{m}$ of both scintillators, as it was confirmed by MCNP6.2
223 simulation. The maximum interaction depth was simulated at $37 \mu\text{m}$ and $45 \mu\text{m}$ for MOF-205
224 and BC-404, respectively. We explain this interaction depth difference from the MOF-205
225 higher density. Due to the detector's resolution and small energy difference between the two
226 alpha rays, it is expected that a single Gaussian-like spectra would be observed. In addition,
227 considering large ionization quenching that are classically encountered with alpha emitters in
228 plastic scintillators (12% of total energy), we expect to see the full absorption peak of the ^{244}Cm
229 alphas around 560 keV .^[20] Results in **Figure 2.A** show that both BC-404 and MOF-205 present
230 a full absorption of ^{244}Cm at channels 18500 and 6500, respectively. However, the light output
231 of the latter was quantified and estimated at 57% the one of BC-404, hence the Gaussian mean
232 value should be expected at higher channel value ($\approx 10,000$). One hypothesis is the loss of
233 photons due to scattering in the MOFs, which is not as transparent as BC-404 plastic scintillator.
234 This was verified by measuring a pellet twice the width. The blue curve of an $800 \mu\text{m}$ thin
235 MOF-205 in **Figure 2.A** shows that the Gaussian peak is very close to the photomultiplier tube
236 noise, thus highlighting the importance of transparency. This is combined with the higher
237 stopping power of MOF-205 as was mentioned before, thus leading to an even more localized
238 interaction (ionization quenching), magnifying the light loss by self-quenching and increasing

239 the pathway for photon transport within this material. To confirm this hypothesis, beta
 240 acquisitions were carried out.



241
 242 **Figure 2. Comparison between scintillation performances of MOF-205 and BC-404.**
 243 Histogram of scintillation data for BC-404 (black), MOF-205_400 μm (red), MOF-205_800 μm
 244 (blue) and 2,6-NDC/BTB in stoichiometric quantity (pink) in presence of A) ^{244}Cm , B) ^{60}Co ,
 245 C) ^{36}Cl and D) $^{90}\text{Sr}/^{90}\text{Y}$. E) ^{241}Am pulse coincidence spectra. Inset in each graph represents the
 246 simulated pulse height spectrum. F) Channel position of the scintillators' response versus
 247 impinging energy.

248
 249 Beta emission spectra are continuous and beta particles present deeper tracks in the matter than
 250 alpha particles, resulting in full or partial energy deposition in the detector, depending of the
 251 incident energy. Three beta radionuclides were used in this study with their main emission as
 252 follows: ^{60}Co ($E_{\beta}^{\text{mean}} = 95 \text{ keV}$, $E_{\beta}^{\text{max}} = 317 \text{ keV}$), ^{36}Cl ($E_{\beta}^{\text{mean}} = 316 \text{ keV}$,
 253 $E_{\beta}^{\text{max}} = 709 \text{ keV}$) and $^{90}\text{Sr}/^{90}\text{Y}$ ($E_{\beta}^{\text{mean}} = 196 \text{ keV}$, $E_{\beta}^{\text{max}} = 546 \text{ keV}$ for ^{90}Sr ,
 254 $E_{\beta}^{\text{mean}} = 927 \text{ keV}$, $E_{\beta}^{\text{max}} = 2279 \text{ keV}$ for ^{90}Y).^[19] Experimental beta acquisition for both BC-
 255 404 and MOF-205 are represented in **Figure 2.B-D** with their respective simulated detection
 256 efficiency. MCNP6.2 simulation stops at the particle-matter interaction and energy deposition,
 257 so do not simulate any luminescence phenomenon nor any light propagation. Therefore, similar
 258 simulation spectra may lead to different experimental spectra, with discrepancies originating
 259 from light generation and propagation. As shown, going from low-energy emitter ^{60}Co to a

260 higher energy emitter ^{36}Cl led to an increasing response in channels, thus in deposited energy.
261 However, comparing ^{36}Cl spectrum with a much higher energy emitter such as $^{90}\text{Sr}/^{90}\text{Y}$, no
262 important change of the spectrum was noticed. This is not surprising considering the high-
263 energy ^{90}Sr beta particles compared to the size of the pellet. Simulated detection efficiency
264 (Inset of **Figure 2.D**) confirms that the generation of less photons comes therefore from a partial
265 energy deposition within the pellet, as both energy deposition spectra are similar in shape and
266 intensity.

267 Moving on to gamma detection possibility, and knowing that the geometry of our scintillators
268 is not ideal for such detection (which requires large detector volume in general), several
269 scintillation spectra were recorded using low-energy gamma emitter such as ^{241}Am
270 ($E_\gamma = 59.5$ keV (36.9%), **Figure 2.E**) and ^{133}Ba ($E_\gamma = 81$ keV (33.3 %) and 356 keV (62.0 %),
271 Figure S6), and compared to simulation. To avoid the possible ^{241}Am alpha interaction, a thin
272 layer of paper was placed between the source and the detector. Simulation shows (Inset of
273 **Figure 2.E**) a noticeable 59.5 keV full absorption peak (PE) that is observable only for MOF-
274 205 due to its higher density than BC-404. Experimentally, this was partially confirmed as BC-
275 404 and MOF-205 spectra showed scintillation response discrepancies. BC-404 is composed of
276 a Compton edge (CE) whereas MOF-205 is composed of a unique Gaussian-type spectrum. We
277 expect that it is a convolution of CE and PE with the corresponding maximum attributed to the
278 59 keV gamma ray. As the considered energy is low and therefore near to the background noise,
279 we used a coincidence assembly to go deeper in our interpretation. Comparison between forms
280 of both spectra (Figure S7) also shows discrepancy. The fact that there are two patterns for
281 MOF-205 is in agreement with our above explanation. So far, the best explanation is that due
282 to the poor resolution of our measurement chain, it is not possible to correctly separate the
283 Compton edge from the PE. Instead, we have a convolution of both corresponding distributions.
284 This trend was also observed for ^{133}Ba (Figure S8). Contrary to the ^{241}Am configuration it is
285 possible to distinguish two contributions. We hypothesized a probable 356 keV full absorption

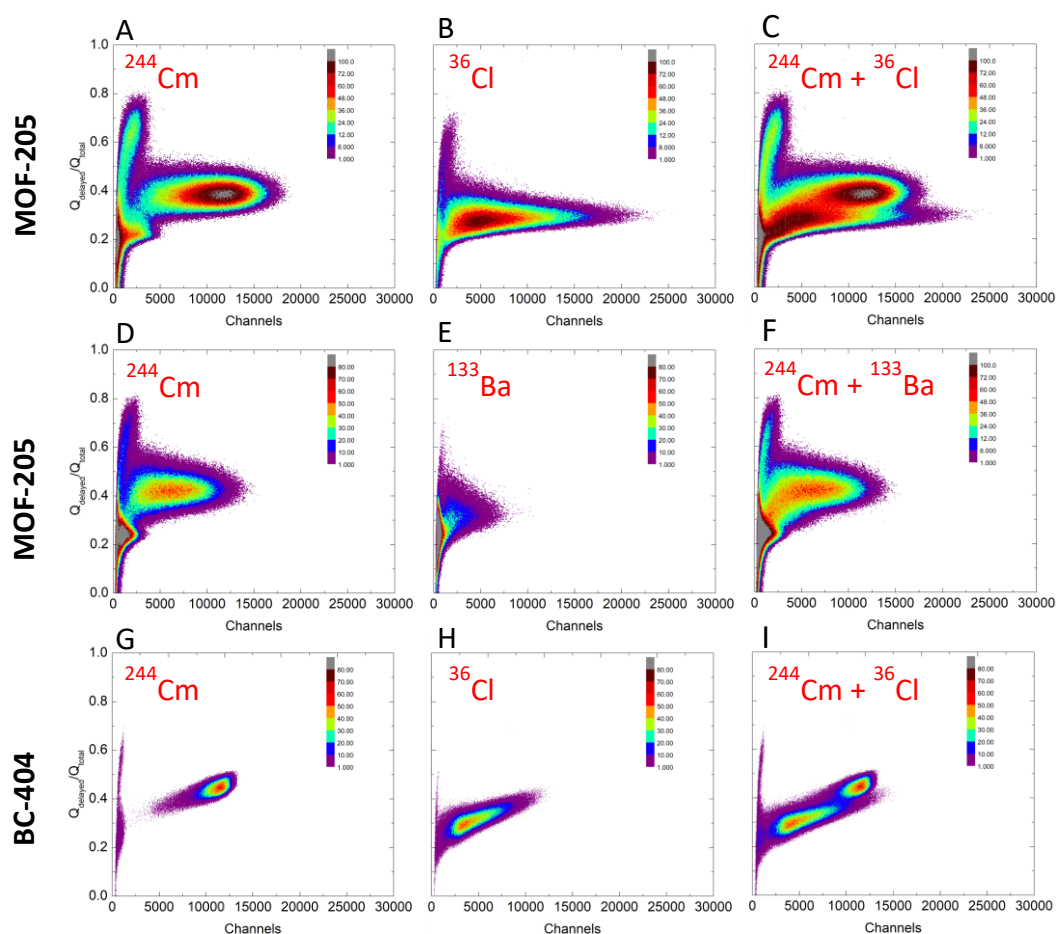
286 peak but it was difficult to investigate and no formal conclusion was drawn even after 10 million
287 pulses recorded. We estimate that the first visible maximum around channels 1900 corresponds
288 to the 81 keV full absorption peak. By comparing the channels between ^{241}Am and ^{133}Ba , these
289 contributions seem to correspond to the two emitted gamma at 81 keV and 356 keV confirming
290 the above hypothesis. To the best of our knowledge, the observation of PE in MOF was never
291 achieved yet and we believe that this was possible in this study due to increased densification.
292 Considering both simulation and experimental data, it was possible to establish a calibration
293 curve by making a parallel with ^{244}Cm alpha spectrum, ^{60}Co and ^{36}Cl beta emitters and gamma
294 emitter such as ^{241}Am and ^{133}Ba . To do so, an energy deposition endpoint for beta distributions
295 was read as the mean value between the first value that reaches zero and the last. For the specific
296 alpha emitter ^{244}Cm , the point was read as the average mean value of the peak. For ^{241}Am and
297 ^{133}Ba gamma emitters, the point was taken into account only for MOF-205 as it presents a full
298 absorption peak and it was read at the maximum of the curve endorsed by simulation. **Figure**
299 **2.F** shows the channels versus the corresponding simulated maximum energy deposition for
300 BC-404 and sintered MOF-205. For BC-404, it is possible to say with confidence that our model
301 fits well as the trend curve passes through the three points with an R^2 factor of 0.9998. This
302 furthers confirms our beta endpoint determination method, which has sufficient precision for
303 an energy calibration curve. Regarding MOF-205 the model looks consistent with the exception
304 of ^{244}Cm . This confirms the previous hypothesis that the auto-quenching for alpha ionization is
305 more important in the MOF than within the BC-404, which means that the output energy is
306 lower than the would be perceived 560 keV. It is also important to note that the trend is linear,
307 even at low energy. However, it is well known that both organic and inorganic scintillator are
308 not linear with the incident energy, this effect appearing below 100 keV.^[21] This observation
309 remains far beyond the scope of this study as the MOF scintillation is still a new field and
310 requires further exploration to draw consistent conclusions.

311 Having explored the scintillation performances of the sintered MOF-205, we tried to challenge
312 the material up a bit with the study of its potential discrimination properties. In particular,
313 alpha/beta and alpha/gamma discrimination were evaluated. It is noteworthy that such
314 properties are not straightforward for all-purpose scintillators and have never been studied in
315 MOF scintillation to the best of our knowledge, even if it was hinted by previous results.^[15]
316 This discrimination is related to higher ionization densities within the material when the
317 incoming particle becomes heavier. This lead to a denser population of excited state, causing
318 increase proximity of triplet state. ^[22] With two neighboring triplet states, annihilation may
319 occur, thus leading to delayed fluorescence paving the way to discrimination between particles
320 of different dE/dx.^[23] MOFs belong to the class of supramolecules that are keen to perform
321 triplet-triplet annihilation,^[24] thus particle discrimination should be effective if properly
322 recorded.

323 As mentioned, two case studies were performed with the same BC-404 and MOF-205 pellets.
324 First is the alpha/beta discrimination, second is the alpha/gamma discrimination. Due to the
325 small size of the MOF-205 scintillator compared with our 2.5 cm diameter sources, experiments
326 were performed sequentially, that is to say alpha then beta or gamma spectra. **Figure 3, top**
327 shows the bidimensional spectra of ²⁴⁴Cm (left), ³⁶Cl (center) and their addition (right). Since
328 the tail of alpha-related pulses is slightly longer than beta- or gamma-related pulses, the
329 integration of the delayed charge over the total charge allows sorting the nature of the excitation
330 that led to scintillation. Such pellet configuration is favorable for this discrimination as the
331 scintillator is intrinsically poorly sensitive to gamma rays and alpha emitters see the full
332 absorption of their energy within the material. But still and as expected, alpha/gamma
333 discrimination using a gamma-emitting ¹³³Ba source was also possible (**Figure 3, middle**). As
334 a visual comparison, alpha/beta discrimination of BC-404 was less pronounced (**Figure 3,**
335 **bottom**), with the two lobes being tilted with a positive slope for an unknown reason. BC-400,
336 a close equivalent to BC-404 was found to display moderate α/β discrimination as well.^[25] In

337 addition, a noticeable Figure of Merit (FOM) of 0.55 was calculated over the full spectrum for
 338 both α/β and α/γ discrimination (Figure S9). Ultimately, fast neutron/gamma discrimination
 339 with MOF-205 was also tested but the results were harsh to interpret, mainly due to the small
 340 size of the material.

341



342

343 **Figure 3.** Pulse Discrimination spectra for various configurations. Left: ^{244}Cm . Center: ^{36}Cl or
 344 ^{133}Ba . Right: superposition of the two precedent spectra. Note that the two ^{244}Cm spectra for
 345 MOF-205 are not identical due to differences in the positioning of the source against the
 346 scintillator. See supporting information for full details.

347

348 3. Conclusion

349 In conclusion, an important advancement in scintillating MOFs characterization is presented
 350 here. Thanks to sintering process, the access to a key parameter such as the light output is now
 351 straightforward if one uses the most appropriate radionuclide (which means alpha or beta
 352 emitters) as the excitation. Here we recommend the use of ^{60}Co or ^{36}Cl as beta source, since

353 their energy is fully absorbed by the material and the stopping range is not too elevated. Thus,
354 a 400 μm thick MOF-205 pellet displayed interesting scintillation properties, an emission
355 wavelength of 409 nm, a mean decay time of 14.3 ns and a scintillation yield 37% the one of
356 anthracene. Both alpha, beta and gamma experimental spectra were supported by MCNP6.2
357 calculations. Our sintered MOF was not fully transparent but the as-prepared pellet was
358 prepared exclusively from MOF-205, as this was our main goal. Pellets potentially prepared
359 with diluted MOF-205 with cubic powder of the same refractive index would lead to materials
360 with better transparency. It is the first time that alpha/beta and alpha/gamma discrimination is
361 qualitatively acknowledged for a MOF. Finally, this study opens a new and exciting research
362 topic. First, we guess that sintered transparent MOFs, achieved for the first time in this work,
363 will be an ongoing and explored field in the next years for optical application mainly. Secondly,
364 this derivative class of metal organic frameworks constitutes a brand new class of scintillator
365 full of opportunities. For instance by using the unique versatility of MOFs and by playing on
366 the composition with heavy metal as nodes and on sintering parameters, we guess that it should
367 be possible to be more sensitive to some ionization and therefore increase the energy response.
368 The goal is to be positioned between organic and inorganic scintillators as a new class of hybrid
369 materials. We hope that this report will be a tremendous input in the field as it brings two new
370 concept relative to the already rich area of MOF: sintering and scintillation discrimination.

371 **Supporting Information**

372 Supporting Information is available from the Wiley Online Library or from the author.

374

375 **Acknowledgements**

376 The Authors wish to thank Pr. Christophe Dujardin for X-ray TCSPC measurement. This
377 project has received funding from the European Union's Horizon 2020 research and innovation
378 programme under Grant Agreement No 899293. This document reflects only the authors' view
379 and the Commission is not responsible for any use that may be made or the information it
380 contains

381 Received: ((will be filled in by the editorial staff))

382 Revised: ((will be filled in by the editorial staff))

383 Published online: ((will be filled in by the editorial staff))

384

-
- [1] a) C. Dujardin, M. Hamel, in *Plastic Scintillators: Chemistry and Applications* (Ed: M. Hamel), Springer-Nature Switzerland AG, **2021**, Ch. 1, pp. 3-33. ; b) G. H. V. Bertrand, M. Hamel, F. Sguerra, *Chem. – Eur. J.* **2014**, *20*, 15660-15685.
- [2] W. C. Röntgen, *Science* **1896**, *3*, 227.
- [3] I. Broser, H. Kallmann, *Z. Naturforsch.* **1947**, *2a*, 642-650.
- [4] a) M. Koshimizu, *Funct. Mater. Lett.* **2020**, *13*, 2030003; b) M. Koshimizu, in *Plastic Scintillators: Chemistry and Applications* (Ed: M. Hamel), Springer-Nature Switzerland AG, **2021**, Ch. 6, pp. 201-222.
- [5] a) O. M. Yaghi, M. O'Keeffe, N. W. Ockwig, H. K. Chae, M. Eddaoudi, J. Kim, *Nature* **2003**, *423*, 705-714; b) G. Ferey, *Chem. Soc. Rev.* **2008**, *37*, 191-214.
- [6] a) L. E. Kreno, K. Leong, O. K. Farha, M.D Allendorf, R. P. Van Duyne, J. T. Hupp *Chemical Reviews* **2012**, *112*(2), 1105-1125; b) W. P. Lustig, S. Mukherjee, N. D. Rudd, A. V. Desai, J. Li, S. K. Ghosh, *Chem. Soc. Rev.* **2017**, *46*, 3242-3285
- [7] a) C. A. Bauer, T. V. Timofeeva, T. B. Settersten, B. D. Patterson, V. H. Liu, B. A. Simmons, M. D. Allendorf, *J. Am. Chem. Soc.* **2007**, *129*, 7136-7144; b) F. P. Doty, C. A. Bauer, A. J. Skulan, P. G. Grant, M. D. Allendorf, *Adv. Mater.* **2009**, *21*, 95-101; c) P. L. Feng, J. V. Branson, K. Hattar, G. Vizkelethy, M. D. Allendorf, F. P. Doty, *Nucl. Instr. Methods A* **2011**, *652*, 295-298; d) S. R. Mathis II, S. T. Golafale, J. Bacsá, A. Steiner, C. W. Ingram, F. P. Doty, E. Auden, K. Hattar, *Dalton Trans.*, **2017**, *46*, 491-500; e) S. R. Mathis II, S. T. Golafale, K. M. Solntsev, C. W. Ingram, *Crystals* **2018**, *8*, 53.
- [8] C. Wang, O. Volotskova, K. Lu, M. Ahmad, C. Sun, L. Xing, W. Lin, *J. Am. Chem. Soc.*, **2014**, *136*, 6171-6174.

-
- [9] J. Perego, I. Villa, A. Pedrini, E. C. Padovani, R. Crapanzano, A. Vedda, C. Dujardin, C. X. Bezuidenhout, S. Bracco, P. E. Sozzani, A. Comotti, L. Gironi, M. Beretta, M. Salomoni, N. Kratochwil, S. Gundacker, E. Auffray, F. Meinardi, A. Monguzzi, *Nat. Photonics* **2021**, *15*, 393-400.
- [10] S. Grasso, M. Biesuz, L. Zoli, G. Taveri, A. I. Duff, D. Ke, A. Jiang, M. J. Reece, *Adv. Appl. Ceram.* **2020**, *119*, 115-143.
- [11] C. J. Werner, J. S. Bull, C. J. Solomon, F. B. Brown, G. W. McKinney, M. E. Rising, D. A. Dixon, R. L. Martz, H. G. Hughes, L. J. Cox, A. J. Zukaitis, J. C. Armstrong, R. A. Forster, L. Casswell, *MCNP Version 6.2 Release Notes*, <http://doi.org/10.2172/1419730>.
- [12] <https://www.crystals.saint-gobain.com/products/organic-scintillation-materials>
- Accessed: July, 2021
- [13] P. L. Feng, J. J. Perry IV, S. Nikodemski, B. W. Jacobs, S. T. Meek, M. D. Allendorf, *J. Am. Chem. Soc.* **2010**, *132*, 15487-15489.
- [14] H. Furukawa, N. Ko, Y. B. Go, N. Aratani, S. B. Choi, E. Choi, A. O. Yazaydin, R. Q. Snurr, M. O’Keeffe, J. Kim, O. M. Yaghi, *Science* **2010**, *329*, 424-428
- [15] J. J. Perry IV, P. L. Feng, S. T. Meek, K. Leong, F. P. Doty, M. D. Allendorf, *J. Mater. Chem* **2012**, *22*, 10235-10248.
- [16] M. Fust, H. Kallmann, *Phys. Rev.* **1955**, *97*, 583-587.
- [17] R. Zacharia, D. Cossement, L. Lafi, R. Chahine, *J. Mater. Chem.* **2010**, *20* (11), 2145–2151.
- [18] a) V. Villemot, M. Hamel, R. B. Pansu, I. Leray, G. H. V. Bertrand, *RSC Adv.* **2020**, *10*, 18418-18422 ; b) A. R. Kshirsagar, X. Blase, C. Attacalite, R. Poloni, *J. Phys. Chem. Lett.* **2021**, *12*, 4045-4051.

-
- [19] M.-M. Bé, V. Chisté, C. Duliéu, M. A. Kellett, X. Mougeot, A. Arinc, V. P. Chechev, N. K. Kuzmenko, T. Kibédi, A. Luca, A. L. Nichols, 2016. Monographie BIPM-5 : Table of Radionucléides. Bureau International des Poids et Mesures. ISBN 978-92- 822-2264-5.
- [20] V. I. Tretyak, *Astropart. Phys.* **2010**, *33*, 40-53.
- [21] W. W. Moses, G. A. Bizarri, R. T. Williams, S. A. Payne, A. N. Vasil'ev, J. Singh, Q. Li, J. Q. Grim, W.-S. Choong, *IEEE Trans. Nucl. Sci.* **2012**, *59*, 2038-2044.
- [22] G. H. V. Bertrand, M. Hamel, S. Normand, F. Sguerra, *Nucl. Instr. Methods A* **2015**, *776*, 114-128.
- [23] D. L. Horrocks, *Rev. Sci. Instrum.* **1963**, *34*, 1035-1040.
- [24] R. Medishetty, J. K. Zaręba, D. Mayer, M. Samoć, R. A. Fischer, *Chem. Soc. Rev.* **2017**, *46*, 4976-5004.
- [25] K. Mitev, C. Dutsov, S. Georgiev, L. Tsankov, T. Boshkova, *IEEE Trans. Nucl. Sci.* **2017**, *64*, 1592-1598.